Soft Matter

Accepted Manuscript

Submitted to Soft Matter

ARTICLE

The role of bond tangency and bond gap in hard-sphere crystallization of chains

Nikos Ch. Karayiannis,*[a] Katerina Foteinopoulou[a] and Manuel Laso[a],

We report results from Monte Carlo simulations on dense packings of linear, freely-jointed chains of hard spheres of uniform size. In contrast to our past studies where bonded spheres along the chain backbone were tangent, in the present work a finite tolerance in the bond is allowed. Bond lengths are allowed to fluctuate in the interval $[\sigma, \sigma + dl]$, where σ is the sphere diameter. We find that bond tolerance affects the phase behaviour of hard-sphere chains, especially in the close vicinity of the melting transition. First, a critical dl^{crit} exists marking the threshold for crystallization, whose value decreases with increasing volume fraction. Second, bond gaps enhance the onset of phase transition by accelerating crystal nucleation and growth. Finally, bond tolerance has an effect on crystal morphologies: in the tangent limit the majority of structures correspond to stack-faulted random hexagonal close packing (r.h.c.p.). However, as bond tolerance increases a wealth of diverse structures can be observed: from single fcc (or hcp) crystallites to random hcp/fcc stackings with multiple directions. By extending the simulations over trillions of MC steps (10^{12}) we are able to observe crystal-crystal transitions and perfection even for entangled polymer chains in accordance to the Ostwald´s rule of stages in crystal polymorphism. Through simple geometric arguments we explain how the presence of rigid or flexible constraints affects crystallization in general atomic and particulate systems. Based on the present results, it can be concluded that proper tuning of bond gaps and of the connectivity network can be a controlling factor for the phase behaviour of model, polymer-based colloidal and granular systems.

1 Introduction

Controlling the phase behaviour of atomic and particulate systems is of extraordinary importance in diverse physical, chemical, engineering and biological processes. How complex molecular structures can be arranged in the bulk or in a confined space and under various processing conditions, is a research topic that keeps receiving persistent scientific attention. This is because the general subject of packing is not limited to the fundamental concepts alone but also applies to a vast number of daily-life applications: from grain silos and transport/storage containers to cosmetics, cell biology and nanofabrication.

From the modelling perspective the most straightforward model to study packing is the one of hard spheres. With respect to theory it is amenable to analytical solutions; from the computational viewpoint it is easily implementable and computationally inexpensive; experimentally it can be mapped into neutral (uncharged) colloids.

The first Monte Carlo (MC)[1] and Molecular Dynamics (MD)[2] simulations focused on such hard-body systems providing pioneering insights on their phase behaviour and packing ability. More than half a century afterwards and the packing of rigid, impenetrable bodies is still in the spotlight of simulation-based research[3-21], with numerous studies focusing on packings of non-spherical and highly complex objects.[22-36] Systems consisting of chains (polymers) fall definitely in this later category. Not only is the shape of macromolecules highly anisotropic, but it fluctuates over time especially in high-temperature melts and dilute solutions. Furthermore, at equilibrium contour paths can be distinctly different from chain to chain. Further contributing parameters to the complexity in modelling and simulation of polymeric systems are i) the very slow dynamics of long macromolecules due to the topological constraints between chains (entanglements)[37-39] that lead to sluggish motion and ii) the large spectrum of characteristic time and length scales that dominate polymer structure, dynamics and rheology[37, 38].

In recent years there has been significant progress in the synthesis and characterisation of colloidal[40, 41] and granular[42-45] polymers. The study of such model realizations offers two significant advantages: first, key concepts such as entanglements and knots can be visualized due to their macroscopic size, and second important factors like molecular

weight, polydispersity, chain architecture and stiffness can be controlled to a desired level.

In parallel to experiments, the packing behaviour of athermal chains can be studied through continuum (off-lattice) simulations. However, due to the very long relaxation times of well-entangled chains conventional simulation techniques cannot effectively explore the phase space of dense polymers, which limits their application to low / intermediate packing densities and to short chains (oligomers).

Solution to this problem has been provided by a Monte Carlo scheme, specially designed to model athermal polymer packings of long chains even close to the jammed state.[46, 47] This MC protocol is built around the configurational bias method[48-51] and chain-connectivity-altering moves[46], inspired by the original end-bridging (EB) and double-bridging (DB) algorithms, which have been successfully applied on polymer melts in atomistic detail.[52, 53] Very extensive MC simulations (in the order of billions (10^9) of steps) of freely-jointed chains of tangent hard spheres of uniform size, allowed us to identify the jammed state of athermal polymer packings,[46, 54] its structural characteristics, and the similarities and differences with the corresponding state of monomeric analogues.[54-56] Through these simulations it was possible to observe all characteristic scaling regimes of the dependence of chain dimensions and of the underlying network of entanglements (primitive paths) on volume fraction.[57-60] Furthermore, it was shown that given enough simulation time and once a critical packing density is reached, freely-jointed chains of tangent hard spheres show a spontaneous, entropy-driven phase transition (crystallization)[54, 61-64] much as their monomeric athermal counterparts do.[2, 10, 14, 19, 20, 65-67] According to simulations at all packing densities above a concentration threshold ($\varphi > 0.56$) random chain packings crystallize into random hexagonal close packed (r.h.c.p.) structures consisting of stack-faulted alternating layers of face-centered cubic (fcc) or hexagonal close-packed (hcp) character with a single stacking direction.[54, 62-64] The ordered morphologies were further characterized by the absence of fivefold defects (twinning), for which an entropic mechanism seems to be responsible.[68]

Accordingly, through computer simulations it has been established that at high volume fractions athermal packings of linear chains show a spontaneous, entropy-driven crystallization like monomeric hard spheres. However, besides the fundamental similarities athermal polymer crystallization shows unique characteristics which are absent or different compared to the phase transition of single (monomeric) hard spheres. First, for freely-jointed chains of *tangent* hard spheres, the density threshold for crystallization ($\varphi_{chains}^M > 0.56$) is substantially higher than the melting transition of monomeric hard spheres ($\varphi_{monomeric}^M \approx 0.545$). In other words, there is a concentration range, the upper border of which is not fully identified, where monatomic hard spheres crystallize but freely-jointed chains of *strictly tangent* hard spheres remain amorphous.[54, 62, 64] In addition, in the tangent limit the prevailing ordered morphology for chains is the r.h.c.p. crystal, while for monomers a wealth of structures can be observed, ranging from single fcc or hcp crystallites to close packed stackings with random directions and twinning planes existing in abundance at crystalline boundaries. Interestingly, similar morphologies were recently found by Ni and Dijikstra[69] in MD simulations of packings of chains with softer bonds.

Motivated by the aforementioned modelling studies[54, 62-64, 69] in the present contribution we analyse, in a systematic fashion through extensive Monte Carlo simulations, the effect of bond constraints on the ability of freely-jointed linear chains of hard spheres of uniform size to crystallize. We investigate the dependence of the melting point, of the established ordered morphologies and of the rate of the disorder-order transition on bond tolerance compared to the tangent limit.

The manuscript is organized as follows: in section 2 we describe the simulation method, the modelled systems and the structural descriptor to gauge local structure. Section 3 contains the results of the present study, their analysis and interpretation. Finally, section 4 summarizes the main findings and conclusions.

2 Simulation Method

Polymers are modelled as linear, freely-jointed chains of hard spheres with uniform diameter, σ. In contrast to past studies,[46, 47, 54-64] where bonded spheres were strictly tangent ($l \equiv \sigma$, l being the bond length) this time bond lengths in the interval $[\sigma, \sigma + dl]$ are allowed, where dl is the parameter that controls the tolerance in bond lengths (maximum bond gap). Obviously, the tangency condition is recovered in the limit $dl \rightarrow 0$. In practice, the parameter dl corresponds to the maximum allowed gap in the bond between two adjacent hard spheres along the chain backbone. It must be noted that the application of bond tolerance does not affect the non-overlapping condition: the distance between sphere centres cannot be less than σ.

Simulation cells are cubic with periodic boundary conditions applied in all dimensions. Generation and equilibration of the polymer chains inside the cells are undertaken by the Monte Carlo (MC) scheme described in detail in Ref.[46]. Not surprisingly the performance of the MC protocol for bond gaps is significantly higher than in the tangent limit. This trend is caused by two factors: i) the configurational bias (CB) pattern employed for all local moves (reptation, intermolecular reptation, rotation, internal libration) results in trial configurations that sample more efficiently the accessible volume left by bond gaps and ii) the acceptance rate of chain-connectivity-altering moves (simplified end-bridging and simplified intramolecular end-bridging)[46] increases, as the number of candidate chains to be bridged rises with bond tolerance. This latter factor also lessens the "shuttling" effect (forward and reverse transitions that annihilate each other) which reduces the equilibration ability of MC algorithms[70] especially at high densities.

Due to the nature of the employed chain-connectivity-altering moves all systems are characterized by polydispersity in molecular lengths, which is properly controlled by casting the simulations in the semi-grand statistical ensemble.[52] As in past studies the distribution of chain lengths is uniform in the interval $[N(1-\Delta), N(1+\Delta)]$, where N is the average chain length, and Δ is the half-width of the length distribution divided by N. For computational expedience and in order to directly compare with previous results most simulations are performed on a system of 100 chains of $N = 12$ ($\Delta = 0.5$) for a total of 1200 hard-sphere monomers. In addition, to check the effect of molecular length and the reproducibility of the main findings two additional systems are simulated: i) 96 chains of $N = 50$ ($\Delta = 0.5$) and ii) 48 chains of $N = 100$ ($\Delta = 0.5$) both with 4800 spheres.
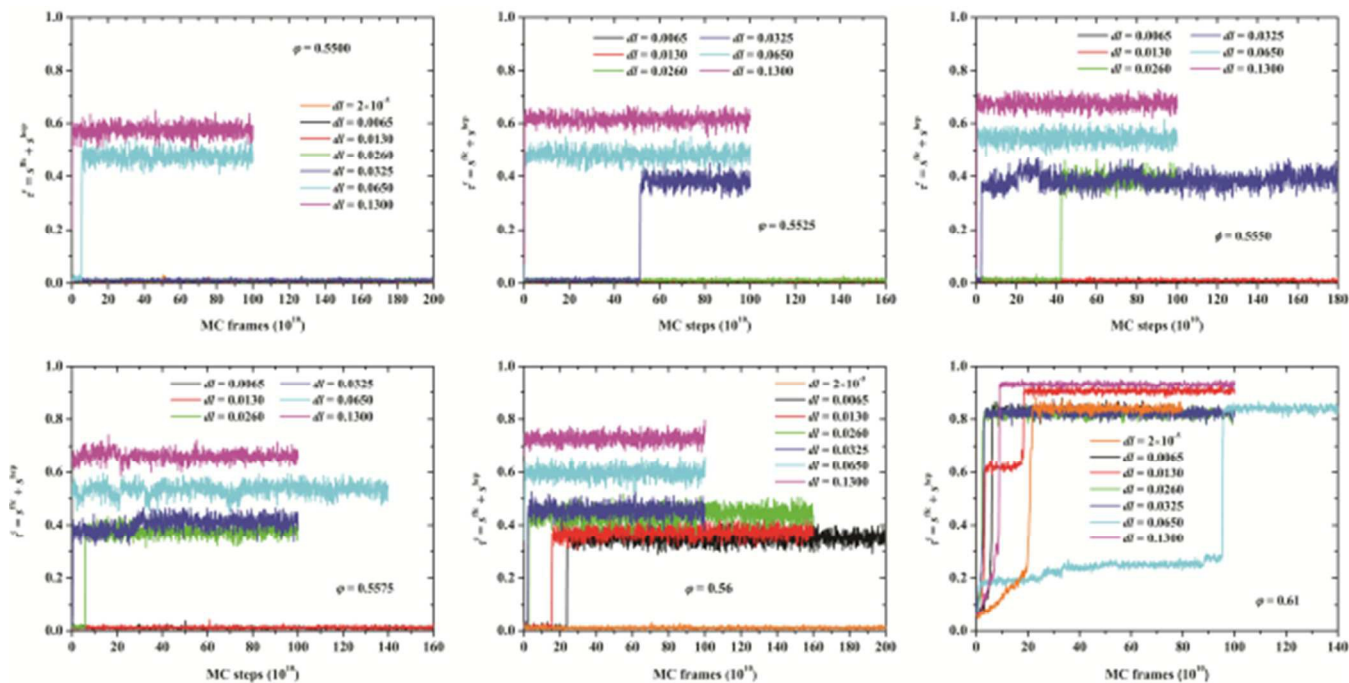
Figure 1. Evolution of crystallinity, τ^c, with MC steps for the *N* = 12 chain system with varied bond tolerance as calculated from the CCE analysis. Upper panel, from left to right: $\varphi = 0.5500$, 0.5525 and 0.5550. Lower panel, from left to right: $\varphi = 0.5575$, 0.5600 and 0.6100.

Initial polymer packings of $N = 12$, corresponding to the tangent limit ($dl \rightarrow 0$), are generated and relaxed at volume fractions of $\varphi = 0.5500$, 0.5525, 0.5550, 0.5575, 0.5600 and 0.6100. Then, representative amorphous configurations at each packing density are selected as starting points for MC simulations with bond gaps. This concentration range is selected so as to study the effect of bond tolerance on the melting transition with respect to the tangent limit and to the monomeric analogues.

In the first stage, the following values of bond tolerance (maximum gap) are employed: dl = 0.0065, 0.0130, 0.0260, 0.0325, 0.0650 and 0.1300. For each value, MC simulations reaching the order of 10^{12} steps are carried out, a simulation length far greater than the ones in our past studies. After analysing the phase behaviour of the modelled systems for the initial set of dl values, whenever necessary, additional values of the bond gap are employed to identify as precisely as possible the critical threshold $dl^{crit}(\varphi)$ for the onset of crystallization (see related discussion in section 3). As in our previous simulations[46] the tangent limit is practically realized by allowing bond tolerances of $dl \approx 2 \times 10^{-5}$ or $dl \approx 10^{-8}$. A comparison of the local and global properties of polymer packings near and above the melting transition and in the vicinity of the MRJ state[55] showed no appreciable difference between the two tolerance values. Based on this and because a bond gap of $dl \approx 2 \times 10^{-5}$ is by more than two orders of magnitude stricter than the bond fluctuations employed in the present work, for all practical purposes this value represents here the tangency condition ($dl \rightarrow 0$). We should note that the range of bond gaps employed here is similar to the ones commonly encountered in experimental realizations, see for example Refs. [44, 45].

Local structure is analysed through the Characteristic Crystallographic Element (CCE) norm[47, 61, 62]. The CCE norm can accurately quantify the orientational and radial similarity of a local environment with respect to a given crystal structure. It is based on the identification of the point group symmetry for each perfect ordered structure[71, 72]. By construction, the CCE norm[19, 20, 47, 54, 56, 60-64, 73] and recent variants[74] are able to distinguish between different crystal structures appearing during disorder-order transitions in general atomic and particulate systems. Details about the mathematical formulation and practical implementation of the CCE-based descriptor can be found elsewhere.[61] Given that in hard-sphere packings the prevailing ordered morphologies correspond to fcc (or hcp) crystals in the present work, as in our past studies, we calculate the CCE norm with respect to the fcc and hcp structures as well as for the non-crystallographic, fivefold symmetry. Based on the value of the corresponding CCE norm a site (sphere monomer) can be labelled as hcp-like, fcc-like, fivefold-like or amorphous (neither hcp, nor fcc, nor fivefold). By adding the fractions of fcc-like (s^{fcc}) and hcp-like (s^{hcp}) sites we can calculate the degree of ordering (crystallinity) simply as $\tau^c = s^{fcc} + s^{hcp}$. By tracking the evolution of the relevant quantities (s^{fcc}, s^{hcp} and τ^c) we can detect a possible onset of crystallization (disorder-order transition). At the level of monomers we can gauge the ordered sites and thus study in detail the nucleation and growth of crystallites[19, 20, 54, 62-64, 73].

System configurations (frames) are recorded every 10^7 steps while the CCE-based analysis is performed every 100 frames. For large bond gaps (see related in discussion in section 3) additional simulations are conducted with much shorter record frequency as crystallization occurs more abruptly the larger the bond gap.

3 Results

3.1 Effect of bond gap on crystallization

As stated in the introduction, present modelling studies are mainly motivated by the difference in the phase behaviour between freely-jointed chains of tangent hard spheres[54, 62-64, 69] and of monomeric hard spheres[19, 20] at and slightly above the melting transition $\varphi_{monomeric}^M$ (see for example Fig. 4 of Ref. [64]). Accordingly, we focus primarily our attention in the concentration range $\varphi \in [0.5500, 0.5600]$ with additional simulations conducted at a higher volume fraction ($\varphi = 0.61$) for comparison purposes. The multiple panels of Fig. 1 show the evolution of crystallinity (τ^c) as a function of MC steps for various values of bond tolerance (dl) at increasing packing densities as obtained for the $N = 12$ system. At the lowest density ($\varphi = 0.5500$) only the two systems with the largest bond gaps ($dl = 0.01300$ and 0.0650), show a sharp first-order, disorder-order transition. Crystallization occurs very early in the MC simulation and the transition is very sharp. However, all other packings remain amorphous, being characterized by very small numbers of hcp and/or fcc sites. As concentration is increased ($\varphi = 0.5525$) the chain system with the third largest bond gap ($dl = 0.0325$) also crystallizes. Therefore, it is evident that as volume fraction increases packings with smaller allowed bond gaps transit to the ordered state. Thus, the effect of bond tolerance on the phase
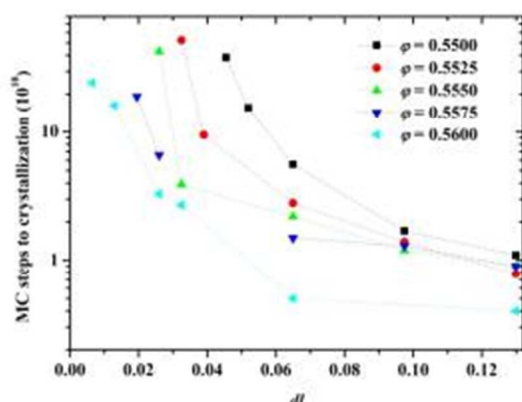
Figure 2. Monte Carlo steps required for the *N* = 12 system to crystallize (in logarithmic scale) as a function of bond tolerance, dl, at various packing densities, φ. Dotted lines connecting simulation points serve as guides for the eye.

behaviour of chain packings declines with increasing volume fraction. The observed trend is manifestly valid as we reach progressively higher densities. For example at $\varphi = 0.56$ bond constraints affect crystallization so weakly that all systems, except the one corresponding to the tangent limit ($dl \rightarrow 0$), show a spontaneous, disorder-order transition.

According to the data of Fig. 1 the following additional conclusions can be drawn with respect to the dependence of crystallization on bond tolerance near the melting transition:
1) the rate of crystallization (nucleation and growth, measured in MC steps) increases as the bond gap widens,
2) the established degree of ordering (crystallinity) decreases as the allowed bond tolerance shrinks,

3) irrespectively of bond tolerance, the disorder-order transition, when it occurs, appears very sharp,
4) there exists a critical bond gap ($dl^{crit}(\varphi)$) above (below) which athermal chains crystallize (remain amorphous).
By comparing the trends in Fig. 1, observed at packing densities near the melting point, with the one obtained at significantly higher volume fraction ($\varphi = 0.6100$), we can conclude that the effect of bond tolerance on crystallization is at maximum very close to the melting transition and weakens as concentration is increased. At sufficiently high volume fractions ($\varphi > 0.5600$) the effect is so weak that polymer packings show spontaneous disorder-order transition even in the tangent limit.
The rate of crystallization can be quantified by calculating the number of MC steps required for the sharp transition. Obviously, the stochastic nature of the MC method, especially when built around "unphysical" chain-connectivity-altering moves like here, prohibits the extraction of "real" dynamical information. In spite of this, MC steps can still be used to quantify the rate with which a reference system, under specific conditions and constraints, reaches the stable phase. Fig. 2 shows the number of MC steps required to reach the stable crystal phase as a function of bond gap at increasing packing densities. Chain assemblies characterized by large bond gaps, are able to crystallize significantly faster than those with smaller tolerance. The trend is systematic and reproducible over all studied packing densities. Furthermore, it is not surprising that in this concentration range $0.55 \leq \varphi \leq 0.56$ denser chain packings crystallize faster than more dilute ones.
Fig. 3 presents the dependence of the degree of ordering (crystallinity) on packing density with increasing bond gaps. First, for the two largest values of bond tolerance ($dl = 0.0650$ and 0.1300) it can be seen that chain packings always crystallize independently of concentration. The corresponding crystallinity of the final morphologies is high: for example for $dl = 0.1300$ and $\varphi = 0.56$ the fraction of ordered sites exceeds $\tau^c > 0.70$. At smaller bond gaps the disorder-order transition
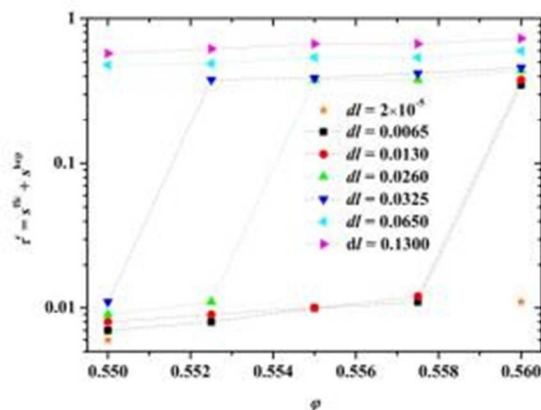
Figure 3. Degree of ordering (crystallinity), τ^c, (in logarithmic scale) as a function of packing density, φ, with varying bond gap, dl, as obtained from MC simulations on the *N* = 12 chain system. Dotted lines connecting simulation points serve as guides for the eye.

depends strongly on the applied combination of dl and φ: for a given bond gap there is a packing density above/below which

chain packings crystallize/remain amorphous. The smaller the bond gap, the higher the volume fraction that has to be reached for crystallization to take place. Eventually, far from the melting point (as established for monomeric hard spheres) most, if not all, of the polymer assemblies crystallize irrespective of the applied bond gap. Similar conclusions can be drawn from Fig. 4 which shows the dependence of crystallinity on bond gap with increasing volume fraction. At a given packing density a critical value of bond gap exists $dl^{crit}(\varphi)$ which, once reached, leads to spontaneous phase transition. The bond gap threshold is clearly a decaying function of packing density as can be seen in Fig. 4.

3.2 Phase diagram of athermal polymer packings

When two successive values of bond tolerance lead to different phase behaviour additional simulations are conducted with intermediate values so as to identify more precisely the
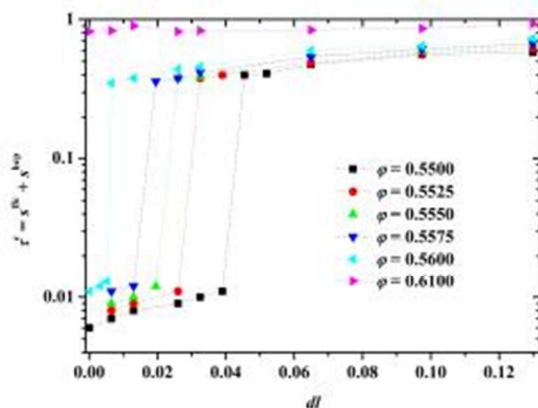
Figure 4. Crystallinity, τ^c, (in logarithmic scale) as a function of bond gap, dl, at increasing packing densities as obtained from MC simulations on the *N* = 12 chain system. Dotted lines connecting simulation points serve as guides for the eye.

threshold value $dl^{crit}(\varphi)$. For example, according to Fig. 1 at $\varphi = 0.5525$ the *N* = 12 system remains amorphous for $dl = 0.0260$ but crystallizes for $dl = 0.0325$. Thus, additional simulations are conducted in the interval $dl \in [0.0260, 0.0325]$ to identify as precisely as possible the threshold value that triggers crystallization at this volume fraction. By combining all available modelling data and by calculating $dl^{crit}(\varphi)$, the phase diagram of athermal polymer packings as a function of volume fraction and bond softness can be formulated, at least for the range of parameters (N, dl and φ) studied here.

Fig. 5 shows the threshold bond gap, $dl^{crit}(\varphi)$, as a function of packing density, marking the boundaries of different phase behaviour: for bond tolerance higher than $dl^{crit}(\varphi)$ ($dl \ge dl^{crit}(\varphi)$) the initially amorphous polymer packing shows spontaneous crystallization, while for $dl < dl^{crit}(\varphi)$ it remains amorphous. At higher densities (for example at $\varphi = 0.61$) bond gaps play no

role in the phase behaviour of athermal chains. Consequently, decreasing bond tolerance in chain packings leads to an increase of the melting point for athermal polymers with respect to monatomic analogues.

From the application perspective, at packing densities near the phase transition, adjusting bond gaps / tangency can be a decisive factor to control the phase behaviour of model polymer-based colloidal or granular systems.

3.3 Semi-crystalline morphologies

As stated in the introduction previous modelling studies have shown that for dense polymer packings ($\varphi \ge 0.58$) of *tangent* hard spheres the resulting crystal structures consist of well-defined, stack-faulted, randomly alternating hcp or fcc layers with a single stacking direction (see for example typical
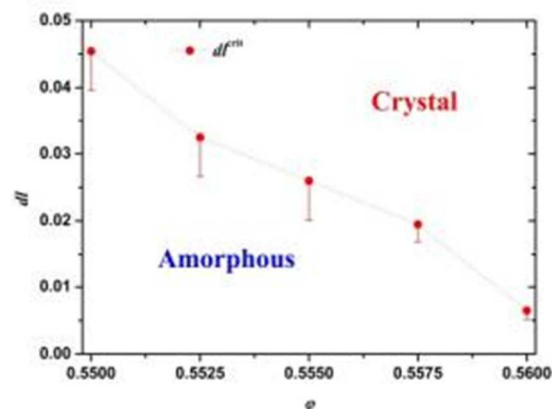
Figure 5. Phase diagram of the *N* = 12 system as a function of packing density, φ, and maximum bond gap, dl. Threshold value $dl^{crit}(\varphi)$ denotes the critical bond gap above which polymer packing shows spontaneous crystallization at a specific volume fraction. Dotted line connecting simulation points serves as guide for the eye. Widths of the one-sided error bars, *w*, correspond to the difference ($w = dl^{crit} - dl^i$) between successive studied values of bond gap (dl^{i+1}, dl^i) for which different phase behaviour is observed ($dl^{crit} = dl^{i+1}$).

snapshots in Fig. 2 of Ref. [62] and in Fig. 3 of Ref. [63]). Such random hexagonal close packed (r.h.c.p.) morphologies are commonly encountered in hard and soft colloidal systems[75-79]. In parallel to experiments, simulations on *monomeric* hard-spheres have revealed a wide spectrum of distinct ordered structures[5, 7, 10, 19, 20, 66, 67, 80]. Ni and Dijkstra[69] in their dynamical simulations on hard-sphere chains with *fluctuating bond lengths* have reported polymer crystal morphologies, which resemble those encountered in monomeric counterparts. Such ordered structures deviate significantly from the r.h.c.p. ones formed abundantly in MC simulations with *tangent* spheres. Questions are thus raised on how the employed methodology (MC vs. MD) and system size, as opposed to the physical parameters (packing density, bond tolerance, and inherent contact network), could in principle affect the formation of specific ordered structured.

Representative crystal morphologies with varying bond tolerance as obtained at the end of the MC simulations at volume fractions $\varphi = 0.5575$ (upper panel) and 0.61 (lower panel) are shown in Fig. 6. For the tangent limit ($dl \rightarrow 0$) the

For single spheres, the fcc crystal is thermodynamically the most stable structure. Its free energy has been found to be, by a very small amount, slightly lower that of the hcp crystal and of all r.h.c.p. structures.[81-83] The thermodynamically stable crystal phase for *chains of tangent hard spheres* is still unknown,
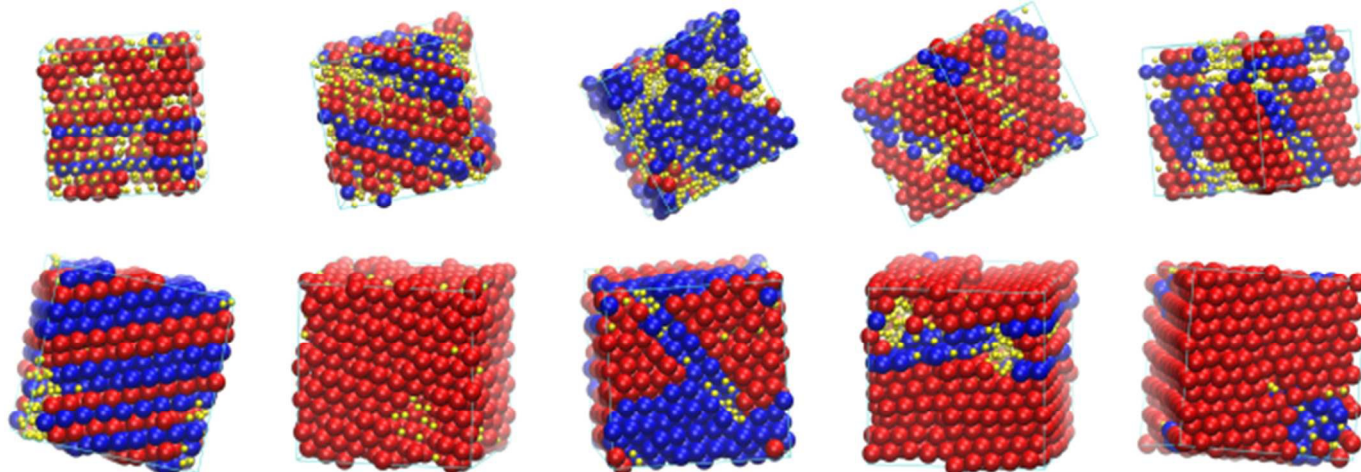
Figure 6. System snapshots as obtained in the end of Monte Carlo simulations. Upper panel: $\varphi = 0.5575$**, from left to right:** $dl = 0.0195$**, 0.0260, 0.0325, 0.0650 and 0.130. Lower panel:** $\varphi = 0.61$**, from left to right:** $dl \rightarrow 0$ **(tangent limit), 0.0130, 0.0325, 0.0650 and 0.130. Spheres are color-coded according to the CCE-norm values: red and blue colours correspond to sites with fcc and hcp similarity, respectively. Amorphous sites are shown in yellow with reduced sphere dimensions (in a ratio of 2:5) for visualization purposes. Image created with the VMD software.**

r.h.c.p structure is obtained in perfect agreement with past MC simulations on athermal chains of tangent spheres. This is clearly demonstrated by the presence of the alternating layers[54, 62-64] of almost exclusive fcc (or hcp) character with a single stacking direction. However, as we depart from the tangency condition a wealth of distinctly different crystal morphologies appears. Primarily, the occurrence of the r.h.c.p morphology diminishes with increasing bond gaps. Out of all crystal structures the fcc-rich morphology appears to be the prevailing one in chains with bond gaps. For example as can be seen in Fig. 6 at $\varphi = 0.61$ and $dl = 0.0130$ all ordered sites are fcc-like and account for more than 91% of the total spheres in the system. Hcp-rich crystals are also encountered but less frequently than fcc-rich ones. Additionally, ordered morphologies with mixed hcp/fcc characters are formed with random orientation and content. The whole set of polymer crystals, established here through MC simulations with allowed bond gaps, is very reminiscent of the ones encountered in simulations of monomeric analogs[5, 7, 10, 19, 20, 66, 67, 79] and in MD-based simulations on athermal[69] and thermal[73] chains with flexible bond lengths. Consequently, it is evident that neither the employed method nor the size of the system could account for the commonness of r.h.c.p-crystals in the tangent limit. For the latter case the transition to a more stable (hcp or fcc) crystal seems impossible due to one hand on the colossal times required due to the hindrance imposed by the tangency condition, and on the other hand because twinning and corresponding morphologies are suppressed due to entropy constraints related to chain conformations.

3.4 Thermodynamic stability of polymer crystals

although the fcc crystal is conjectured to be the one. At maximum compactness ($\varphi \approx 0.7404$) the main contribution to the free energy difference Δf between hcp and fcc is related to the chain conformational entropy which is given by the logarithm of the number of self-avoiding random walks on the fully occupied hcp and fcc lattices. This number scales with chain length N as $A\mu^N N^{(\gamma-1)}$ [84], where γ is a universal constant, equal for hcp and fcc, and A and μ (the connective constant) are lattice specific. Limited numerical evidence indicates that $\left(A\mu^N\right)_{\{hcp\}} < \left(A\mu^N\right)_{\{fcc\}}$ for all chains lengths, and thus chain connectivity further increases the stability of the fcc crystal phase with respect to the hcp one.

Accordingly, the frequent occurrence of fcc-rich morphologies in MC simulations of athermal packings with bond tolerance is not surprising. In parallel, a plethora of different chain crystals can also emerge as evident from the snapshots of Fig. 6. This crystal polymorphism is in accordance to Ostwald´s rule of stages according to which the first ordered structure to be established is the least stable one, i.e. the one with the closest similarity to the amorphous phase. Successive crystal-crystal transformations would eventually lead to the most stable structure.[85] While valid for a range of physical systems[86, 87] the multi-stage phase rule is not universal nor theoretically founded, lacking also microscopic features incorporated in recent models.[88]

It is interesting to explore whether present MC simulations could provide insights with respect to the concept of multi-stage phase transition and of structural perfection in athermal polymer packings. To this end we study how the individual hcp (s^{hcp}) and fcc (s^{fcc}) fractions evolve with time (MC steps). A possible change in their ratio, or evidently in their sum (τ^c),
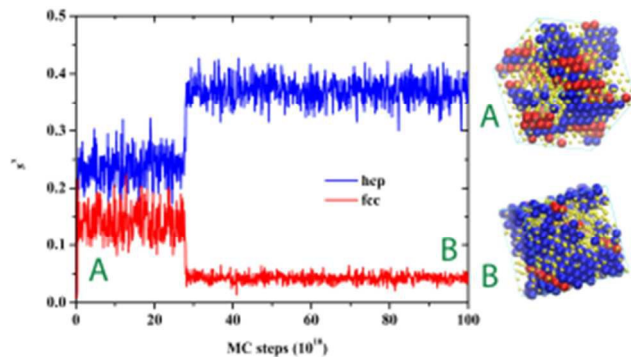
Figure 7. Left: Evolution of the fraction of sites with hcp (s^{hcp}) and fcc (s^{fcc}) similarity as a function of MC steps as obtained from MC simulations on the *N* = 12 system at $\varphi = 0.5575$ and $dl = 0.0325$. Right: System configurations at (A) 5×10^{10} and (B) 80×10^{10} MC steps. Spheres are color-coded according to the pattern of Fig. 6.

could be a strong indication of a possible crystal-crystal transformation. Such an argument can be supported through
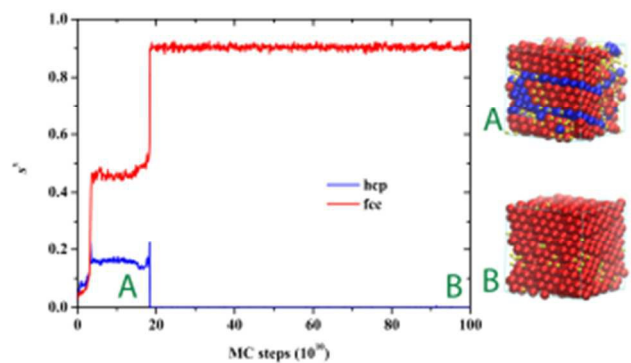
Figure 8. Same as in Fig. 7 but at $\varphi = 0.61$ and $dl = 0.0130$.

visual inspection of the corresponding system configurations. Figs. 7 and 8 show how the hcp and fcc fractions evolve with MC steps for the *N* = 12 system at $\varphi = 0.5575$ ($dl = 0.0325$) and at $\varphi = 0.61$ ($dl = 0.0130$), respectively. At $\varphi = 0.5575$ ($dl = 0.0325$) the initial disorder-order transition, which occurs very early in both cases, leads the system to a semi-crystalline morphology, which persists for a significant simulation period, where the hcp and fcc populations are comparable. However at

approximately 27×10^{10} MC steps, a second, equally-sharp transition takes place. As a consequence the fraction of hcp-like sites increases appreciably at the expense of the fcc population, which leads to a small net increase in total crystallinity (as can be verified by the curve in lower left panel of Fig. 1). According to the system snapshots, shown in the right panel of Fig. 7, the ordered chain packing transits from a mixed, randomly-oriented hcp/fcc crystal to an hcp-abundant one with very few clusters of fcc sites. Similar trends are observed in Fig. 8, for the combination of $\varphi = 0.61$ and $dl = 0.0130$. However, here the crystal-crystal transition is more drastic: first, there is a substantial increase in crystallinity (this can be also deduced from the corresponding curve in the lower right panel of Fig. 1), and second in the resulting stable crystal there are no traces of hcp-like sites. According to the systems snapshots in the right panel of Fig. 8 the initial fcc-rich morphology, with very well-defined fcc regions being bounded by hcp layers, is eventually transformed into an almost perfect, single fcc crystal (τ^{c} 0.91 , s^{fcc} 0.91). Similar crystal – crystal transitions are also observed for other chain packings with bond tolerance (not shown here). In some cases such stage transitions are accompanied by an increase in the degree of ordering while in some others, there is no detectable change in τ^{c} but only in the relative hcp and fcc fractions.

In contrast, athermal polymers in the tangent limit remain in the r.h.c.p ordered state without showing any further transformations to a thermodynamically more stable crystal morphology (mainly the hcp or the fcc crystals) for the whole simulation time. It should be noted that the total duration of a MC simulations exceeds by at least two to three orders of magnitude the time required for crystallization.

3.5 Crystallization of entangled athermal chains

Due to computational constraints the majority of the simulations are carried out for the *N* = 12 system. These relative short chains (oligomers) are not fully representative of polymeric behaviour. This is mainly due to the fact that chains are so short that topological constraints between chains (physical entanglements) are rare. Secondly, in oligomeric species the population of chain ends is elevated compared to the one of internal monomers. This, in turn, affects the applied bond constraints: in the *N* = 12 system approximately 16% of the sphere population corresponds to chain ends. If we consider the *N* = 50 and 100 systems this fraction drops to significantly lower levels: 4% and 2%, respectively.

The results presented in the previous sections are expected to be qualitatively valid independently of the average molecular length, since the latter should affect primarily the rate of crystallization and to a much lesser degree the established crystallinity rather than the general trends.

Soft Matter Accepted Manuscript

In order to support the aforementioned statements we embark on MC simulations with significantly longer chains than in our past works:[54, 62-64] $N = 50$ and 100 (with a total of 4800 hard spheres) at packing densities of $\varphi = 0.56$, 0.58, 0.60 and 0.61
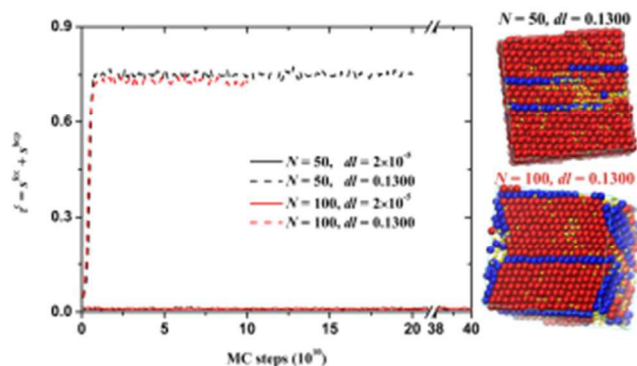
Figure 9. Left panel: Degree of ordering, τ^c, as a function of MC steps for the N = 50 and 100 systems at $\varphi = 0.56$ in the tangent limit (solid lines) and for $dl = 0.1300$ (dashed lines). Right panel: System configurations at the end of MC simulations for $dl = 0.1300$. Spheres are color-coded as in Fig. 6.

both in the tangent limit and with varying bond gaps. Regular simulations are conducted starting from initial amorphous (random) chain configurations. In parallel, crystals corresponding to the tangent limit serve as initial configurations for successive MC simulations with increasing bond tolerance. Fig. 9 shows the evolution of the degree of ordering versus MC steps for the $N = 50$ and 100 systems at $\varphi = 0.56$ in the tangent limit ($dl \rightarrow 0$) and for the largest allowed bond gap ($dl = 0.1300$).

The qualitative trends observed for the oligomeric system ($N = 12$) are fully confirmed also by the significantly longer $N = 50$

and 100 systems. In the tangent limit, both systems remain amorphous with a very small, almost negligible, fraction of ordered sites; in agreement with the trends observed for the $N = 12$ and 24 systems as shown here (Fig. 1) and in past studies[62-64]. In sharp contrast, once we increase the bond gap ($dl = 0.1300$) both chain assemblies transit very rapidly to the ordered state. The crystallization rate appears to be unaffected by the average chain length and is slower than the one observed for the $N = 12$ system. This trend is expected given the different system size since more MC steps are required to sample the extended sphere sample. The right panel of Fig. 9 hosts snapshots of the ordered morphologies as obtained at the end of the MC simulations for bond gaps. For $N = 50$ the crystal is predominately of fcc character interrupted by two tilted hcp-like layers. For $N = 100$ the presence of a twinned fcc crystal bounded by planes of hcp similarity can be clearly identified, an ordered morphology which is very reminiscent of corresponding ones observed for monomeric analogues[10].

Fig. 10 shows the evolution of crystallinity with MC steps for the $N = 50$ and 100 systems at $\varphi = 0.58$, initially in the tangent limit ($dl \rightarrow 0$). At this volume fraction long chains crystallize as oligomers do. In fact, for tangent spheres the longer chain ($N = 100$) shows slower ordering rate than the shorter one ($N = 50$), characterized by the same total number of monomers. This behaviour is in contrast with the one observed at $\varphi = 0.56$ for bond gaps (Fig. 9) suggesting that by allowing tolerance in bond lengths the effect of chain length on crystal nucleation and growth becomes significantly weaker if not non-existent.

As can be seen in the right panel of Fig. 10 both systems, in the

Figure 10. Left panel: Crystallinity as a function of MC steps for the N = 50 and 100 systems at $\varphi = 0.58$. Simulation data in the tangent limit ($dl = 2 \times 10^{-5}$) are shown with solid lines. At 30×10^{10} MC steps, as marked by the vertical dotted line, (ordered) configurations with tangent spheres serve as initial configurations for MC simulations with a bond gap of $dl = 0.1300$ (dashed lines). Right panel: ordered chain configurations as obtained in the end of simulations. Spheres are color-coded according to the pattern of Fig. 6.

tangent limit, result in polymer crystals of r.h.c.p morphology where the thickness of the pure fcc (or hcp) components can reach 5-6 sequential layers. Once the chain assembly reaches the stable crystal phase, additional simulations are carried out increasing the allowed bond gap from $dl = 2 \times 10^{-5}$ to 0.1300. The corresponding curves are added in Fig. 10 and thus the effect of bond gap can be directly compared with the behaviour

in the tangent limit. First, once bonds are allowed to fluctuate a substantial increase is observed in the degree of ordering: from τ^c 0.57 for tangent bonds to 0.87 for $dl = 0.1300$. The increase in crystallinity occurs so rapidly that the transition cannot be captured with the current record frequency in the MC trajectory. Second, the behaviour between the two systems ($N = 50$ and 100) is practically indistinguishable once bond tolerance of this amplitude is allowed. Finally, with respect to the established crystals, bond gaps lead to perfection of the established r.h.c.p morphologies as the majority of sites, previously characterized by disordered local environment, are now incorporated into the hcp/fcc layers. The morphology of the polymer crystal, as obtained in the tangent limit, remains basically unaltered, however the size of the ordered domain grows significantly.

3.6 The role of bond tangency and bond gap in athermal chain crystallization

In dense chain packings the local environment at the level of sphere monomers undergoes significant re-arrangements in order to maximize the local density or equivalently to reduce the unoccupied local volume. This trend is obvious in the bending and torsion angle distributions which develop clear and sharp maxima corresponding to characteristic sphere arrangements.[56] For example the most prominent bending angle, that at 60°, practically corresponds to an equilateral triangle which is the locally densest possible conformation in successive sphere triplets along the chain backbone. Likewise,
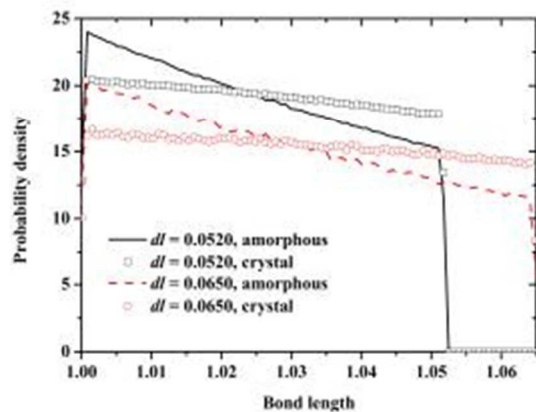
Figure 11. Distribution of bond lengths for the *N* = 12 system at $\varphi = 0.5500$ **with maximum bond gaps being set at** $dl = 0.0520$ **(black color) and 0.0650 (red color). Lines correspond to the initial amorphous packing early in the simulation, while scattered open symbols correspond to the semicrystal phase in the end of the simulation.** $\tau^c \square$ **0.38 and 0.48 for** $dl = 0.0520$ **and 0.0650, respectively.**

with respect to bond lengths, tangency ($dl \to 0$) maximizes the occupied volume between any two spheres, while any bond length tolerance leads to inter-sphere gaps ($dl > 0$) which decrease local density. However, the tendency of chain assemblies to maximize their local density is opposed by the

tendency of athermal chains to crystallize. In other words the inclination towards maximum local packing in the metastable branch, which leads to the MRJ state, competes against the entropically-favored, ordered space filling that leads to the hcp/fcc crystal phase. This competition is not exclusive to chain packings but rather a common characteristic shared with monomeric analogues. Fig. 11 shows the bond length distribution for the $N = 12$ system at $\varphi = 0.5500$ with $dl = 0.0520$ and 0.0650 both in the initial amorphous (early in the simulation) and in the final crystal (in the end of the simulation) phases. We should remind here that there is no potential dependent on bond length, except from the condition that it must lie in the allowed range $[\sigma, \sigma + dl]$. The curves of Fig. 11 reveal that as the system transits to the crystal phase the distribution of bond lengths becomes more uniform and its mean shifts to a larger value. The change in bond lengths is significant especially if we take into account that in the ordered phase more than half of the sphere population remain amorphous, thus not requiring structural re-arrangements with respect to bond distances. Crystallization clearly proceeds by forcing the bonded atoms around a given, reference one to move to greater distances compared to tangency. In other words, the local environment becomes more dilute and more spatially homogeneous and isotropic, so that the spheres around the reference one adopt farther positions but at the same time more symmetric ones in the crystallographic sense. In fact this (localized) push-off of neighbours leads to the local environment being orientationally *and* radially more similar to the fcc (or hcp) structures.
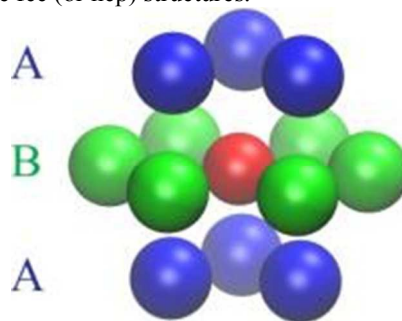
Figure 12. Crystallographically perfect hexagonal close-packed (hcp) structure with alternating ABA stacks. Reference sphere is coloured in red, neighbour spheres are color-coded according to the stack they belong.

Nevertheless, bond constraints in chain packings, which are absent in monatomic systems, add some complication to the picture. Not surprisingly, the simulation results just presented show that the influence of bond constraints is strongest in the case of zero bond tolerance (tangency).

To understand the role of tangency in athermal chain crystallization we will focus on the effect of the inherent contact network (as imposed by the tangency condition) on the formation of a *crystallographically perfect* hcp structure (identical arguments can be employed for the fcc crystal with the corresponding crystallographic operations and elements). In the following discussion we consider the limit of linear long chains where the population of chains ends is insignificant compared to internal monomers so that any sphere is effectively bonded to two other monomers.

The first coordination shell around a reference sphere (marked in red) in the hcp structure with the ABA alternating stacks is shown in Fig. 12 with spheres being coloured according to the stack they belong to. The tangency condition dictates that the reference sphere be in contact with two spheres that belong to the same chain and, automatically, to the coordination shell. Consequently, if a *perfect hcp* crystal is to be formed, the number of possible connectivity patterns for the tangent bonds is limited. Different cases can be identified depending on which planes are spanned by the bonds between the reference sphere and its two tangent neighbors along the chain. Fig. 13 shows all distinct possibilities (not counting others that are just rotated or reflected versions of those shown). In case I) both tangent spheres are located in the upper A layer; in II) one is in the upper A, the other in the lower A layer; in III) both are in the B layer, and in IV) one is in the A, the other in the B layer. For each of these possibilities we can further identify sub-cases depending on the bending angle formed by the bond vectors. For example the subpatterns of case III, from left to right, are characterized by bending angles of 180, 60 and 120°, respectively. Based on the above, for the formation of a *crystallographically perfect* hcp environment in the tangent limit, the following conditions must be fulfilled: in cases I, II and III a total of 6 spheres should be tangent to the reference sphere leading to a coordination number of (at least) 6. In case IV the corresponding kissing number increases to 12 as all spheres in the ABA stacks must be tangent to the reference sphere.

Thus, it is evident that the tangency condition imposes spatial constraints for the formation of the hcp (and similarly of the fcc) structure which, if fulfilled, should lead to a significant increase in the local density. In fact, case IV leads to the perfect, close-packed hcp crystal with a coordination number of 12 and of the maximum possible packing density (≈ 0.7404). It is clear that the formation of such *ordered and efficiently packed* structure with a density far above the bulk density is very unlikely at intermediate concentrations, especially in the vicinity of the melting point.

Above melting for an amorphous packing the critical condition for the formation of crystallites is the crystallographic symmetry fulfilment. In the case of tangent bonds, if it is to be obeyed for the hcp and fcc structures, this condition leads to (locally) densely packed contact networks with no fewer than 6 spheres. Furthermore, ordered structures following especially the pattern of case IV with 12 contact neighbors are encountered very rarely if at all at intermediate packing densities.

As concentration increases, the effect of tangency condition, described above, decreases because monomers lie closer and the contact network becomes progressively richer. Thus, it is much easier to find (no less than) six monomers around a reference sphere that fulfill the geometric arrangements of cases I – III. Case IV with its kissing number of 12 should still remain the most demanding connectivity pattern and thus the least frequently encountered one.

Once a critical packing density is reached the average contact network becomes sufficiently populated so that the tangency condition does not affect anymore chain crystallization. According to our simulation data for the $N = 12, 24, 50$ and 100 systems this density lies in the range $0.56 < \varphi \le 0.58$.

The analogous effect, when bond gaps are allowed, can be readily understood as a relaxation of the tangency condition: the geometric arguments presented in Fig. 12 do not require kissing numbers of 6 or 12 but rather symmetrically placed

monomers within a tolerance of dl. The higher the value of dl the easier for the neighbours around a reference sphere to adopt proper configurations in orientational and radial terms. Furthermore, since the two bonds can in principle possess different lengths (dl_1 and dl_2), case IV is significantly relaxed
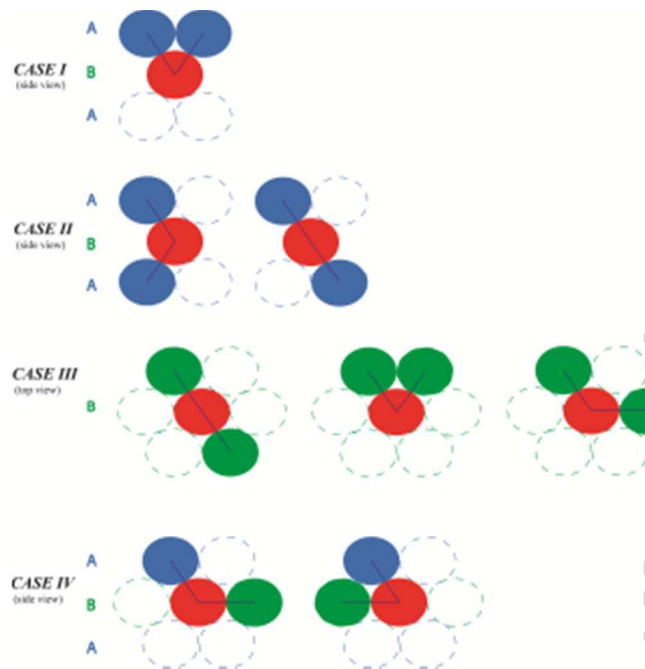
Figure 13. Possible connectivity combinations in an hcp structure subject to tangency condition. Bonded neighbours are shown in filled circles. Empty circles with dashed outline indicate candidate sphere positions for the formation of perfect hcp structure. Cases I, II and IV are shown in side view while case III in top view. Not all spheres in the ABA stacks are shown for better clarity. All depicted cases correspond to the same hcp crystal of Fig. 12. For each case different connectivity patterns are dictated by the bending angle between the bond vectors.

as dl_1 dictates for example the symmetry positions in plane A and dl_2 in plane B without any cross-correlation.

Accordingly, it is not surprising that at all packing densities the larger the allowed bond gap the easier (and the faster) the chain assembly transits to the ordered state. Additionally, this further explains the crystal perfection observed (Fig. 10) once we allow bond gaps in a crystal originally formed under the tangency condition: the existing crystallites remain unaffected but more sites are able to form ordered structures due to the allowed bond gaps.

We should note that the simple geometric arguments we have presented and the corresponding condition on the contact network (mainly to consist of 6 or 12 spheres depending on the case) for the tangent limit correspond to the perfect hcp crystal. In practice, non-ideal crystals are formed as the local environment around each site in an originally amorphous medium is distorted compared to the ideal structure. Still, such simple arguments remain manifestly valid: monomers which are tangent to the reference sphere will greatly reduce the degree of the hcp/fcc similarity except if the rest of neighbours are also very close to the reference sphere.

Finally, with respect to oligomeric systems a brief comment on the effect of chain ends on crystallization is in order. If the reference sphere is a chain end then the tangency condition is limited to a single bond. The single tangency condition does not affect cases I-III, at least with respect to the formation of a perfect hcp crystal. Instead, it eliminates the most geometrically-demanding case (IV). Furthermore, in all cases it leads to a reduced crystallographic error (CCE norm) in the calculation of a distorted local structure. Thus, crystal nucleation is expected to occur easier at chain ends rather than in internal hard-sphere monomers. From the technical perspective, the combination of chain-connectivity-altering moves with localized ones, that displace chain ends (like reptation or rotation), constantly creates new crystallization pathways in the course of a MC simulation. A chain-connectivity-altering move within a step can change the identity of a sphere from internal mer to chain end, while successive localized moves can further displace the sphere and its neighboring atoms, as needed to create an hcp- or fcc-like local structure. The complete set of possible variations of a perfect hcp environment for linear chains in the tangent limit or in the presence of bond gaps can be found in Fig. 14. The difference in the local density imposed by the tangency condition and the corresponding contact network (as shown in Fig. 13 and analysed in related discussion) with respect to the general, constraint-free hcp structure is pretty evident.
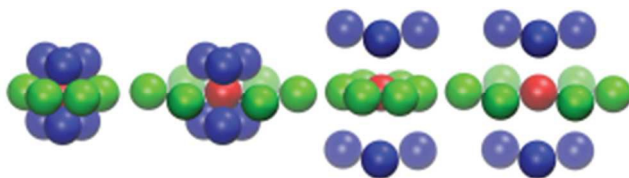
Figure 14. Variations of crystallographically perfect hexagonal close packed (hcp) structures. From left to right: a) coordination number of 12 with atoms in planes A and B being tangent to reference atom (case *IV* in Fig. 13), b) coordination number of 6 with atoms in planes A being tangent to reference atom (cases *I* and *II* in Fig. 13), c) coordination number of 6 with atoms in plane B being tangent to the reference atom (case *III* in Fig. 13). Variations a)-c) imposed by the tangency condition can be directly compared with the general hcp crystal structure in the presence of bond gaps (right most panel).

4 Conclusions

We have presented results from extensive MC simulations on athermal polymer packing with tangent bonds and with bond tolerance. In agreement with past studies[54, 62-64, 69] we find that allowing gaps in bonds has a profound effect on the phase behaviour of chain assemblies in the close vicinity of the melting transition (of monatomic hard spheres). The smaller the bond tolerance, the more difficult for the chains to crystallize and the lower the disorder-order transition rate. Furthermore, the established crystal morphologies are affected by bond gaps: in the tangent limit the resulting structure is the random hexagonal close packed (rhcp) crystal, free of fivefold defects. With increasing bond tolerance chains can transit to

thermodynamically more stable crystals, mainly the hcp and fcc ones. Based on present simulation data the phase diagram of athermal polymers can be established as a function of packing density and of bond tolerance.

Extensions to systems with longer and entangled chains fully confirmed findings obtained from oligomers. Crystal perfection can be observed when we allow bond gaps in r.h.c.p-like morphologies in the tangent limit.

Simple geometric arguments, related to the connectivity patterns in the tangent limit and in the presence of bond gaps can be used to explain the effect of bond constraints on the phase behaviour of chain packings. It is concluded that the tangency condition requires the presence of a (local) contact network with at least 6 kissing sites. Practically, tangency results in a strict radial condition according to which the spheres must be symmetrically placed and densely packed. The latter is not favoured at intermediate concentrations. As we increase packing density the effect of tangency is reduced because the contact network becomes richer (the inter-sphere distances are reduced).

The proposed geometric argument is not limited to polymeric systems; it can be employed to explain the phase behaviour of any atomic or particulate system with an inherent contact network, or with explicit holonomic constraints.

From the practical perspective, insights can be gained on how the phase behaviour and packing ability of synthesized granular and colloidal polymers can be manipulated by controlling the inherent bond network; in branched polymers, in blends of chains and monomers and in chains with specific rigid bond constraints l_{fix} ($l_{\text{fix}} > \sigma$). The latter case is expected to have the opposite effect of the tangency condition: at high packing densities the presence of nano-voids, that cannot be filled, could annihilate crystallization as tangency does at lower packing densities.

In the light of the spatial constraints described above it is expected that confinement (for example in the form of impenetrable flat plates) should significantly affect the crystallization of chain molecules in the vicinity of walls due to enhanced concentration which in principle should partially reduce or even eliminate the effect of bond constraints.

Based on the above, significant differences are expected in the crystal nucleation and growth of highly non-linear polymers (for example with short and long branches or with star chains) with respect to linear counterparts. Results from systematic simulation studies on such systems and of their blends in the bulk and under confinement will be presented in future studies.

Notes and references

ᵃ Institute of Optoelectronics and Microsystems (ISOM) and ETSII, Polytechnic University of Madrid (UPM), Madrid, 28028, Spain. E-mail: nkarayiannis@etsii.upm.es

† Throughout the manuscript, time, rather than having a physical meaning, corresponds to number of Monte Carlo steps.

1. N. Metropolis, A. W. Rosenbluth, M. N. Rosenbluth, A. H. Teller and E. Teller, *J. Chem. Phys.*, 1953, **21**, 1087-1092.
2. B. J. Alder and T. E. Wainwright, *J. Chem. Phys.*, 1957, **27**, 1208-1209.
3. S. Punnathanam and P. A. Monson, *J. Chem. Phys.*, 2006, **125**, 024508.
4. H. Y. Chen and H. R. Ma, *J. Chem. Phys.*, 2006, **125**, 024510.
5. A. V. Anikeenko, N. N. Medvedev, A. Bezrukov and D. Stoyan, *J. Non-Cryst. Solids*, 2007, **353**, 3545-3549.
6. C. Song, P. Wang and H. A. Makse, *Nature*, 2008, **453**, 629-632.
7. T. Kawasaki and H. Tanaka, *Proc. Natl. Acad. Sci. U. S. A.*, 2010, **107**, 14036-14041.
8. A. Donev, S. Torquato and F. H. Stillinger, *Phys. Rev. E*, 2005, **71**, 011105.
9. J. A. van Meel, D. Frenkel and P. Charbonneau, *Phys. Rev. E*, 2009, **79**, 030201.
10. B. O'Malley and I. Snook, *Phys. Rev. Lett.*, 2003, **90**, 085702.
11. B. O'Malley and I. Snook, *J. Chem. Phys.*, 2005, **123**, 054511.
12. A. Donev, F. H. Stillinger and S. Torquato, *Phys. Rev. Lett.*, 2005, **95**, 090604.
13. A. V. Anikeenko and N. N. Medvedev, *Phys. Rev. Lett.*, 2007, **98**, 235504.
14. E. Zaccarelli, C. Valeriani, E. Sanz, W. C. K. Poon, M. E. Cates and P. N. Pusey, *Phys. Rev. Lett.*, 2009, **103**, 135704.
15. N. Arkus, V. N. Manoharan and M. P. Brenner, *Phys. Rev. Lett.*, 2009, **103**, 118303.
16. G. N. Meng, N. Arkus, M. P. Brenner and V. N. Manoharan, *Science*, 2010, **327**, 560-563.
17. K. N. Pham, A. M. Puertas, J. Bergenholtz, S. U. Egelhaaf, A. Moussaid, P. N. Pusey, A. B. Schofield, M. E. Cates, M. Fuchs and W. C. K. Poon, *Science*, 2002, **296**, 104-106.
18. R. S. Hoy, J. Harwayne-Gidansky and C. S. O'Hern, *Phys. Rev. E*, 2012, **85**, 051403.
19. N. C. Karayiannis, R. Malshe, J. J. de Pablo and M. Laso, *Phys. Rev. E*, 2011, **83**, 061505.
20. N. C. Karayiannis, R. Malshe, M. Kroger, J. J. de Pablo and M. Laso, *Soft Matter*, 2012, **8**, 844-858.
21. G. Brambilla, D. El Masri, M. Pierno, L. Berthier, L. Cipelletti, G. Petekidis and A. B. Schofield, *Phys. Rev. Lett.*, 2009, **102**, 085703.
22. S. Torquato and Y. Jiao, *Phys. Rev. E*, 2010, **82**, 061302.
23. H. Altendorf and D. Jeulin, *Phys. Rev. E*, 2011, **83**, 041804.
24. Z. A. Tian, K. J. Dong and A. B. Yu, *Phys. Rev. E*, 2014, **89**, 032202.
25. A. Donev, I. Cisse, D. Sachs, E. Variano, F. H. Stillinger, R. Connelly, S. Torquato and P. M. Chaikin, *Science*, 2004, **303**, 990-993.
26. A. Donev, F. H. Stillinger and S. Torquato, *Phys. Rev. Lett.*, 2006, **96**, 225502.
27. Y. Jiao, F. H. Stillinger and S. Torquato, *Phys. Rev. E*, 2009, **79**, 041309.
28. S. Torquato and Y. Jiao, *Nature*, 2009, **460**, 876-U109.
29. Y. Jiao and S. Torquato, *Phys. Rev. E*, 2011, **84**, 041309.
30. S. Atkinson, Y. Jiao and S. Torquato, *Phys. Rev. E*, 2012, **86**, 031302.
31. N. Xu, J. Blawzdziewicz and C. S. O'Hern, *Phys. Rev. E*, 2005, **71**, 061306.
32. Z. Zeravcic, N. Xu, A. J. Liu, S. R. Nagel and W. van Saarloos, *Epl*, 2009, **87**, 26001.
33. A. Haji-Akbari, E. R. Chen, M. Engel and S. C. Glotzer, *Phys. Rev. E*, 2013, **88**, 012127.
34. T. Chen, Z. Zhang and S. C. Glotzer, *Langmuir*, 2007, **23**, 6598-6605.
35. T. Chen, Z. Zhang and S. C. Glotzer, *Proc. Natl. Acad. Sci. U. S. A.*, 2007, **104**, 717-722.
36. D. Frenkel, H. N. W. Lekkerkerker and A. Stroobants, *Nature*, 1988, **332**, 822-823.
37. P. G. deGennes, *Scaling Concepts in Polymer physics*, Cornell University Press, Ithaca, 1980.
38. M. Doi and S. F. Edwards, *The theory of polymer Dynamics*, Clarendon Press, Oxford, 1988.
39. T. C. B. McLeish, *Adv. Phys.*, 2002, **51**, 1379-1527.
40. H. R. Vutukuri, A. F. Demirors, B. Peng, P. D. J. van Oostrum, A. Imhof and A. van Blaaderen, *Angew. Chem. Int. Ed.*, 2012, **51**, 11249-11253.
41. S. Sacanna, W. T. M. Irvine, P. M. Chaikin and D. J. Pine, *Nature*, 2010, **464**, 575-578.
42. E. Brown, A. Nasto, A. G. Athanassiadis and H. M. Jaeger, *Phys. Rev. Lett.*, 2012, **108**, 108302.
43. L.-N. Zou, X. Cheng, M. L. Rivers, H. M. Jaeger and S. R. Nagel, *Science*, 2009, **326**, 408-410.
44. K. Safford, Y. Kantor, M. Kardar and A. Kudrolli, *Phys. Rev. E*, 2009, **79**, 061304.
45. E. Ben-Naim, Z. A. Daya, P. Vorobieff and R. E. Ecke, *Phys. Rev. Lett.*, 2001, **86**, 1414-1417.
46. N. C. Karayiannis and M. Laso, *Macromolecules*, 2008, **41**, 1537-1551.
47. N. C. Karayiannis and M. Laso, *Phys. Rev. Lett.*, 2008, **100**, 050602.
48. J. I. Siepmann and D. Frenkel, *Mol. Phys.*, 1992, **75**, 59-70.
49. J. J. de Pablo, M. Laso and U. W. Suter, *J. Chem. Phys.*, 1992, **96**, 6157-6162.
50. J. J. de Pablo, M. Laso and U. W. Suter, *J. Chem. Phys.*, 1992, **96**, 2395-2403.
51. M. Laso, J. J. de Pablo and U. W. Suter, *J. Chem. Phys.*, 1992, **97**, 2817-2819.
52. P. V. K. Pant and D. N. Theodorou, *Macromolecules*, 1995, **28**, 7224-7234.
53. N. C. Karayiannis, V. G. Mavrantzas and D. N. Theodorou, *Phys. Rev. Lett.*, 2002, **88**, 105503.
54. N. C. Karayiannis, K. Foteinopoulou and M. Laso, *Philos. Mag.*, 2013, **93**, 4108-4131.
55. N. C. Karayiannis, K. Foteinopoulou and M. Laso, *Phys. Rev. E*, 2009, **80**, 011307.
56. N. C. Karayiannis, K. Foteinopoulou and M. Laso, *J. Chem. Phys.*, 2009, **130**, 164908.
57. K. Foteinopoulou, N. C. Karayiannis, M. Laso, M. Kroger and M. L. Mansfield, *Phys. Rev. Lett.*, 2008, **101**, 265702.
58. M. Laso and N. C. Karayiannis, *J. Chem. Phys.*, 2008, **128**, 174901.

59. N. C. Karayiannis and M. Kroger, *Int. J. Mol. Sci.*, 2009, **10**, 5054-5089.

60. M. Laso, N. C. Karayiannis, K. Foteinopoulou, M. L. Mansfield and M. Kroger, *Soft Matter*, 2009, **5**, 1762-1770.

61. N. C. Karayiannis, K. Foteinopoulou and M. Laso, *J. Chem. Phys.*, 2009, **130**, 074704.

62. N. C. Karayiannis, K. Foteinopoulou and M. Laso, *Phys. Rev. Lett.*, 2009, **103**, 045703.

63. N. C. Karayiannis, K. Foteinopoulou, C. F. Abrams and M. Laso, *Soft Matter*, 2010, **6**, 2160-2173.

64. N. C. Karayiannis, K. Foteinopoulou and M. Laso, *Int. J. Mol. Sci.*, 2013, **14**, 332-358.

65. S. C. Mau and D. A. Huse, *Phys. Rev. E*, 1999, **59**, 4396-4401.

66. V. Luchnikov, A. Gervois, P. Richard, L. Oger and J. P. Troadec, *J. Mol. Liq.*, 2002, **96-7**, 185-194.

67. S. Auer and D. Frenkel, *Nature*, 2001, **409**, 1020-1023.

68. N. C. Karayiannis, K. Foteinopoulou and M. Laso, *Symmetry*, 2014, **6**, 758-780.

69. R. Ni and M. Dijkstra, *Soft Matter*, 2013, **9**, 365-369.

70. N. C. Karayiannis, A. E. Giannousaki and V. G. Mavrantzas, *J. Chem. Phys.*, 2003, **118**, 2451-2454.

71. W. Borchard-Ott, *Kristallographie*, Springer Verlag, Berlin, 2002.

72. C. Giacovazzo, H. L. Monaco, G. Artioli, D. Viterbo, G. Ferraris, G. Gilli, G. Zanotti and M. Gatti, *Fundamentals of Crystallography*, Oxford Science, Oxford, 2005.

73. R. S. Hoy and N. C. Karayiannis, *Phys. Rev. E*, 2013, **88**, 012601.

74. C. Wu, N. C. Karayiannis, M. Laso, D. Qu, Q. Luo and J. Shen, *Acta Materialia* 2014, **72**, 229-238.

75. P. N. Pusey, W. Vanmegen, P. Bartlett, B. J. Ackerson, J. G. Rarity and S. M. Underwood, *Phys. Rev. Lett.*, 1989, **63**, 2753-2756.

76. J. X. Zhu, M. Li, R. Rogers, W. Meyer, R. H. Ottewill, W. B. Russell and P. M. Chaikin, *Nature*, 1997, **387**, 883-885.

77. N. A. M. Verhaegh, J. S. Vanduijneveldt, A. Vanblaaderen and H. N. W. Lekkerkerker, *J. Chem. Phys.*, 1995, **102**, 1416-1421.

78. A. V. Petukhov, I. P. Dolbnya, D. Aarts, G. J. Vroege and H. N. W. Lekkerkerker, *Phys. Rev. Lett.*, 2003, **90**, 028304.

79. W. K. Kegel and J. K. G. Dhont, *J. Chem. Phys.*, 2000, **112**, 3431-3436.

80. N. N. Medvedev, A. Bezrukov and D. Shtoyan, *J. Struct. Chem.*, 2004, **45**, S23-S30.

81. L. V. Woodcock, *Nature*, 1997, **385**, 141-143.

82. P. G. Bolhuis, D. Frenkel, S. C. Mau and D. A. Huse, *Nature*, 1997, **388**, 235-236.

83. A. D. Bruce, N. B. Wilding and G. J. Ackland, *Phys. Rev. Lett.*, 1997, **79**, 3002-3005.

84. N. Madras and G. Slade, *The Self-Avoiding Walk*, Birkhauser, Boston, 1996.

85. W. Ostwald, *Z. Phys. Chem.* , 1897, **22**, 289-330.

86. P. R. ten Wolde and D. Frenkel, *Phys. Chem. Chem. Phys.*, 1999, **1**, 2191-2196.

87. Z. Tavassoli and R. P. Sear, *J. Chem. Phys.*, 2002, **116**, 5066-5072.

88. L. O. Hedges and S. Whitelam, *J. Chem. Phys.*, 2011, **135**, 164902.

The role of bond tangency and bond gap in hard sphere crystallization of chains

Nikos Ch. Karayiannis, Katerina Foteinopoulou, and Manuel Laso

Graphical Abstract
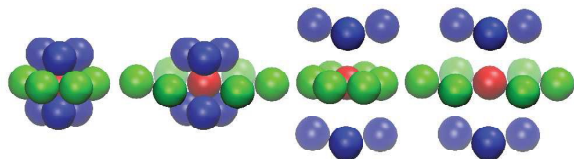
Textual Abstract

We analyze the effect of bond tangency and of bond gaps on the crystallization of chains of hard spheres.